Selection and gene flow shape genomic islands that control floral guides

Hugo Tavares[a,1], Annabel Whibley[a], David L. Field[b,c], Desmond Bradley[a], Matthew Couchman[a], Lucy Copsey[a], Joane Elleouet[a], Monique Burrus[d], Christophe Andalo[d], Miaomiao Li[e,f,g], Qun Li[e,f], Yongbiao Xue[e,f,g,h], Alexandra B. Rebocho[a], Nicolas H. Barton[b,2], and Enrico Coen[a,2]

[a]Department of Cell and Developmental Biology, John Innes Centre, NR4 7UH Norwich NR4 7UH, United Kingdom; [b]Institute of Science and Technology Austria, 3400 Klosterneuburg, Austria; [c]Department of Botany and Biodiversity Research, Faculty of Life Sciences, University of Vienna, A-1030 Vienna, Austria; [d]Laboratoire Evolution et Diversité Biologique, UMR 5174 CNRS–Université Paul Sabatier, 31062 Toulouse Cédex 9, France; [e]State Key Laboratory of Molecular Developmental Biology, Institute of Genetics and Developmental Biology, Chinese Academy of Sciences, 100101 Beijing, China; [f]National Center for Plant Gene Research, Chinese Academy of Sciences, 100101 Beijing, China [g]School of Life Sciences, University of Chinese Academy of Sciences, 100190 Beijing, China; and [h]Beijing Institute of Genomics, Chinese Academy of Sciences, 100101 Beijing, China

Genomes of closely-related species or populations often display localized regions of enhanced relative sequence divergence, termed genomic islands. It has been proposed that these islands arise through selective sweeps and/or barriers to gene flow. Here, we genetically dissect a genomic island that controls flower color pattern differences between two subspecies of *Antirrhinum majus*, *A.m.striatum* and *A.m.pseudomajus*, and relate it to clinal variation across a natural hybrid zone. We show that selective sweeps likely raised relative divergence at two tightly-linked *MYB*-like transcription factors, leading to distinct flower patterns in the two subspecies. The two patterns provide alternate floral guides and create a strong barrier to gene flow where populations come into contact. This barrier affects the selected flower color genes and tightly-linked loci, but does not extend outside of this domain, allowing gene flow to lower relative divergence for the rest of the chromosome. Thus, both selective sweeps and barriers to gene flow play a role in shaping genomic islands: sweeps cause elevation in relative divergence, while heterogeneous gene flow flattens the surrounding "sea," making the island of divergence stand out. By showing how selective sweeps establish alternative adaptive phenotypes that lead to barriers to gene flow, our study sheds light on possible mechanisms leading to reproductive isolation and speciation.

hybrid zone | *Antirrhinum* | genomic island | selective sweep | speciation

Genome scans of closely-related species or populations have revealed "genomic islands" as peaks of high relative sequence divergence (F_{st}) that stand out against a lower "sea" of divergence (1–5). The causes of genomic islands remain unclear, but they have been suggested to contain key loci involved in local adaptation and/or reproductive isolation (6). However, their significance for speciation with or without gene flow between populations is a matter of debate (6–9). One hypothesis is that gene flow is unimpeded across most of the genome, reducing between-population diversity, except for loci under divergent selection and loci in close physical linkage to selected loci (8). Another hypothesis is that genomic islands reflect selective sweeps, where specific alleles are driven to high frequency, thus reducing within-population diversity (7, 9, 10). These two hypotheses are typically presented as alternatives, although they are not mutually exclusive: both barriers to gene flow and selective sweeps may play a role. Here, we determine how these processes contribute to a genomic island that controls floral differences between two subspecies of *Antirrhinum majus*: *A.m.striatum* and *A.m.pseudomajus*. This system has the advantage of being genetically tractable and having a hybrid zone that allows selection and gene flow to be analyzed in nature (11, 12).

Antirrhinum has closed flowers that are prised open by pollinating bees. *A.m.striatum* and *A.m.pseudomajus* exhibit two different floral patterns that signpost the bee entry point (Fig. 1 *A* and *B*). *A.m.striatum* flowers have restricted veins of magenta anthocyanin on upper petals, which contrast against a yellow aurone background (Fig. 1*A*). *A.m.pseudomajus* exhibits a complementary pattern, with a patch of yellow at the bee entry point on lower petals contrasted against magenta (Fig. 1*B*). Yellow patterning is controlled by *SULF* (12). Here we focus on control of magenta by the *ROSEA* (*ROS*) and *ELUTA* (*EL*) loci (13–15). The advantage of studying these loci is that they are tightly linked, allowing variation in intervening regions to provide insights into evolutionary forces. A further locus influencing magenta pigmentation pattern is *VENOSA*, which promotes magenta in dorsal veins (14). Many natural accessions carry *VEN* alleles, while the cultivated species *A. majus* used for genetic analysis typically carries *ven*, allowing its effects to be seen in genetic crosses.

Flowers homozygous for recessive alleles at all three loci (*ros el ven*) have very weak magenta pigmentation (Fig. 1*C*). Introduction of *VEN* leads to magenta overlying the veins of dorsal petals (Fig. 1*D*), whereas introduction of *ROS* leads to strong magenta throughout the corolla (Fig. 1*E*). The semidominant *EL* allele restricts the magenta conferred by *VEN* and *ROS* to lie over the bee entry point (Fig. 1 *F* and *G*). The *ROS* locus contains three *MYB*-like transcription factors, *ROS1*, *ROS2*, and *ROS3*, with ∼90% protein sequence identity in the MYB domain. So far, only *ROS1* and *ROS2* have been functionally characterized, with *ROS1* exerting the major control on anthocyanin levels and pattern (14).

Significance

Populations often show "islands of divergence" in the genome. Analysis of divergence between subspecies of *Antirrhinum* that differ in flower color patterns shows that sharp peaks in relative divergence occur at two causal loci. The island is shaped by a combination of gene flow and multiple selective sweeps, showing how divergence and barriers between populations can arise and be maintained.

Fig. 1. Genetics of flower color. Flowers of *A.m.striatum* (*A, ros^s/ros^s EL^s/EL^s sulf^s/sulf^s*) and *A.m.pseudomajus* (*B, ROS^p/ROS^p el^p/el^p SULF^p/SULF^p*). Each panel shows face view (*Left*), inside of dorsal petals (*Right*), and closeup (*Bottom*). Arrowheads highlight dorsal (*A*) and ventral (*B*) patterns. (*C–G*) Progeny of crosses between plants from the hybrid zone and lines of *A. majus*, illustrating phenotype of various allele combinations. All are *SULF^m/-* or *SULF^p/-*. (*C*) *ros^s/ros^d el^p/el^m ve/ve* gives a flower with pale magenta color on petal periphery. (*D*) *ros^s/ros^s el^p/el^p VE/-* has flowers with magenta veins because of *VE*. (*E*) *ROS^p/ROS^p el^p/el^p* gives strong magenta throughout the flower due to *ROS* allele (*venosa* genotype unknown). (*F*) *ros^s/ros^s EL^s/EL^s VE/-* has vein pigment restricted to a central region. (*G*) *ROS^p/ROS^p EL^s/EL^s ve/ve* giving a restricted pattern of pigmentation compared with *E*. (*H*) *ROS*/ROS* el^p/el^p ve/ve* have spread magenta but of weaker intensity than conferred by *ROS* (compare with *E*). Allele superscripts and abbreviations used in figure legend: *, recombinant; *d, dorsea* (mutant in *A. majus* background); *m, majus; p, A.m.pseudomajus; s, A.m.striatum; X/-,* unknown whether homozygous or heterozygous for dominant allele *X*.

EL is tightly linked to *ROS* but has not been previously isolated (11, 14). Selection at *ROS* has been inferred from analysis of a hybrid zone between *A.m.striatum* and *A.m.pseudomajus*: both magenta pigmentation and *ROS* allele frequencies show sharp clines, ~1 km wide, whereas markers >5 cM from *ROS* show more uniform allele frequency distributions (11).

Flower color differences between *A.m.striatum* and *A.m.pseudomajus* are unlikely to be maintained by adaptation to local conditions, as there are no clear differences in environment or pollinators across the hybrid zone (16). Rather, hybrids and recombinants may be selected against because their flower patterns are less effective as signposts for bee entry than the parental patterns (12, 17) and possibly because bees favor the commonest local phenotype (18–20). This situation is similar to how wing color pattern differences are maintained in *Heliconius* butterflies (21–23). *Heliconius* genes interact to generate distinct color patterns, which signal distastefulness to predators (24). Several patterns can deter *Heliconius* predators, just as several can highlight *Antirrhinum* flower entry. Sharp clines in *Heliconius* are maintained because hybrid phenotypes are less

effective (23) and because the commonest pattern is fitter (22). Genomic islands are observed at the wing pattern loci and are particularly striking near hybrid zones (2, 21, 25).

Here we combine analysis of pooled DNA sequences and SNP frequencies from across the hybrid zone between *A.m.striatum* and *A.m.pseudomajus*, with genetic and gene expression analysis of parental and recombinant genotypes. We pinpoint the loci responsible for differences in anthocyanin flower color pattern and show that they underlie genomic islands of high F_{st}. Through examination of sequence variation around and between the islands, combined with simulations, we show that the islands reflect multiple selective sweeps, which raise relative divergence locally. The sweeps create a barrier to gene flow, which leads to the islands standing out from the genomic sea. Thus, both selective sweeps and barriers to gene flow play key roles in the creation and shaping of genomic islands.

Results and Discussion

Patterns of Differentiation and Diversity. To determine the pattern of sequence diversity around the *ROS* locus, we estimated relative sequence divergence, F_{st}, between *A.m.striatum* and *A.m.pseudomajus* by sequencing pools of ~50 individuals sampled from either side of the hybrid zone, with the centers of the pools separated by ~2.5 km (*SI Appendix*, Fig. S1 and Table S1) (26). SNP analysis of individuals showed that these pools provided good estimates of allele frequencies (*SI Appendix*, Fig. S2). Low F_{st} was observed throughout the genome except for regions with elevated F_{st} on chromosomes 2, 4, and 6 (Fig. 2*A*). We focused our analysis on the peak on chromosome 6 as this is where the *ROS* locus maps (Fig. 2*B*). At a finer scale, three sharp peaks were found in the *ROS* region superimposed on a broader region of increased F_{st} (Fig. 2*C*). The left peak included *ROS1* and *ROS2* (*ROS3* is in a region of lower F_{st}). These F_{st} peaks were not observed between pools from the same side of the hybrid zone (Fig. 2 *D* and *E* and *SI Appendix*, Fig. S3). Thus, the F_{st} peaks in the *ROS* region represent genomic islands of divergence between *A.m.striatum* and *A.m.pseudomajus*.

F_{st} is defined as $(\pi_b - \pi_w)/(\pi_b + \pi_w)$, where π_b (also known as d_{xy}) and π_w are the absolute pairwise divergence between and within populations, respectively (7). An increase in F_{st} can therefore be due to an increase in π_b, a decrease in π_w, or a combination of the two. Plotting π_b against π_w revealed that for the F_{st} peak lying over the *ROS* locus (left peak), π_w is low, whereas π_b is similar to that across the rest of the genome (Fig. 2 *F* and *G*; red points, Fig. 3*A*). The *ROS/EL* region does not fall in a region of reduced recombination (*SI Appendix*, Fig. S4), so low recombination cannot explain the observed reduced diversity, unlike in other cases (27). Instead, reduced diversity at *ROS* is likely due to fixation of one or more favorable mutations (selective sweeps). The right F_{st} peak, ~150 kb downstream of *ROS*, is also primarily due to a decrease in π_w (lower green points, Fig. 3*A*). π_w is reduced in both populations, for both the left and right peaks, implying at least four sweeps (i.e., at two loci for each of the two populations). By contrast, the middle peak does not have low π_w but, rather, relatively high π_b (light blue points, Fig. 3*A*). The middle peak is absent or reduced in some population comparisons (detailed below), suggesting that selective sweeps were not involved in generating it. The above results thus indicate that only the left and right F_{st} peaks arose through selective sweeps.

Mapping the Causal Loci. To determine whether the regions subject to selective sweeps had phenotypic effects, we introgressed *ros EL* from *A.m.striatum* into *A. majus* (*ROS el*) and genotyped F2 populations. Recombinants were backcrossed or self-pollinated to determine their homozygous phenotypes (Fig. 4 *B–F*). Regions causing the *ROS* phenotype mapped to the left F_{st} peak, while the *EL* phenotype mapped to the middle and/or right F_{st} peaks. The limits of *ROS* and *EL* were further refined by crossing plants heterozygous for *ros EL* (from *A.m.striatum*) and *ROS el* (from *A.m.pseudomajus* or *A. majus*) to a *ros el/ros el* line. Screening 10,261 progeny yielded 26 *ROS EL* recombinants, mapping *EL* to an interval of ~50 kb (Fig. 4*G*), below the right F_{st} peak. The map distance between *ROS* and *EL* was 0.5 cM, corresponding to ~3 cM/Mbp, which is of the

EVOLUTION

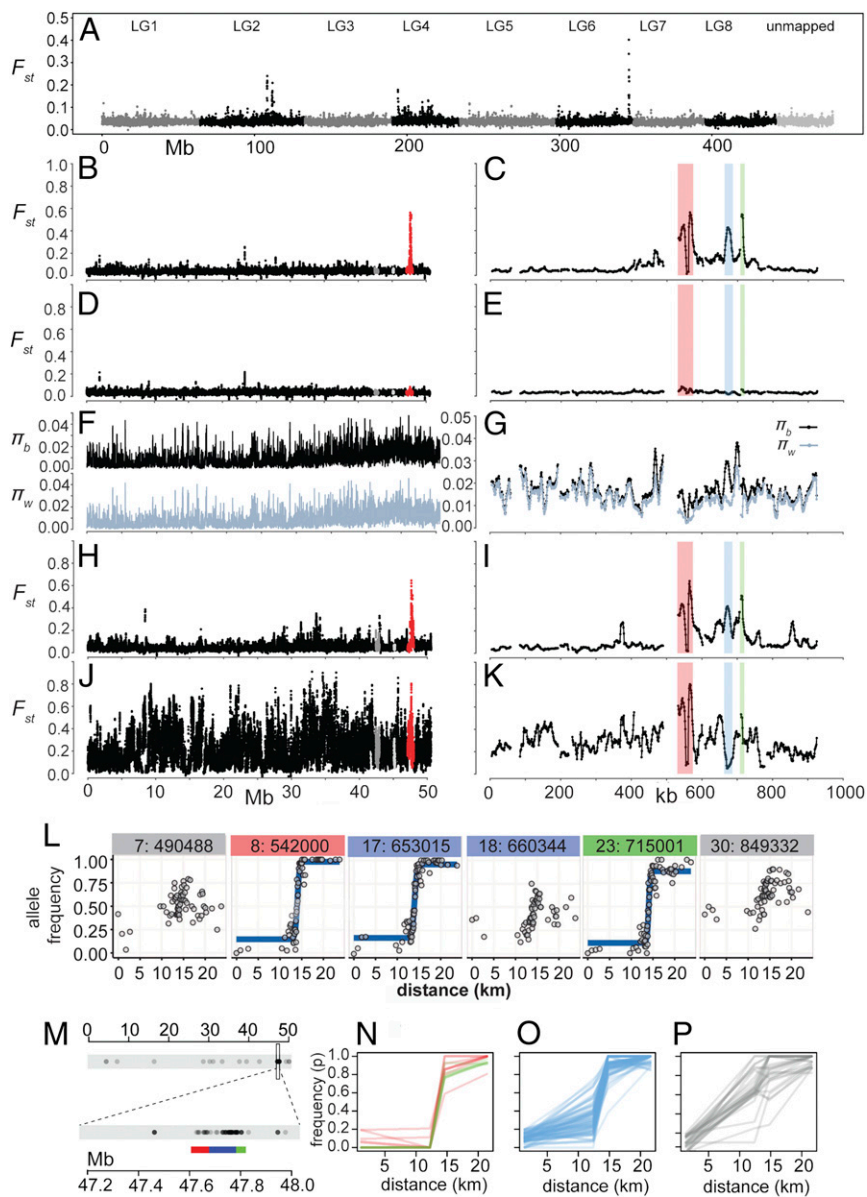**Fig. 2.** Divergence between *A.m.striatum* and *A.m. pseudomajus*. (*A*) F_{st} comparisons between pools of *A.m.striatum* and *A.m.pseudomajus* populations either side of a hybrid zone (YP1 vs. MP2) and ~2.5 km apart across the whole genome summarized in 50-kb windows with a 25-kb step size. (*B*) Same pools as *A* at 10-kb window resolution with 1-kb step size for chromosome 6. A region of high F_{st} is within a ~930-kb scaffold containing the *ROS* gene (red). Linked scaffolds contain *DICHOTOMA* (dark gray) and *PALLIDA* (light gray). (*C*) Closeup of region of high F_{st} at *ROS* comprising three peaks: left (red, 530–575 kb), middle (blue, 663–687 kb), and right (green, 707–720 kb on the *ROS* scaffold). The ~930-kb scaffold corresponds to positions 47.088–48.015 Mb on chromosome 6. (*D* and *E*) Pools from the same side of the hybrid zone (YP1 vs. YP2, both *A.m.striatum*, 0.2 km apart). (*F* and *G*) π_b and mean π_w for the same sequence data as used in *B* and *C*. (*H* and *I*) Pools sampled from populations either side of the hybrid zone (YP4 vs. MP11), ~20 km apart. (*J* and *K*) Pools sampled from remote populations (~100 km apart, ML vs. CIN). (*L*) Clines for selected SNPs genotyped across the hybrid zone population. Headings denote the SNP identifier and position within the *ROS* 930-kb scaffold. (*M*) Distribution of 115 differential SNPs showing allele frequency differences >0.8 between the outer pools (YP4 and MP11) and coverage of 20–200× in all pools. Enlarged *Inset* shows regions corresponding to *ROS* peak (red), intervening region (blue), and *EL* peak (green). (*N*) SNP allele frequencies in the pools for eight differential SNPs within the *ROS* peak (red) and six within the *EL* peak (green) exhibit clines centered at the hybrid zone. (*O*) Most of the 74 SNPs located within the interval between the *ROS* and *EL* peaks, plotted in blue, exhibit clines centered at the hybrid zone. (*P*) SNP frequencies outside the *ROS* and *EL* peaks derive from flanking regions on the *ROS* superscaffold (*n* = 13) or elsewhere on LG6 (*n* = 14).

same order as the genome-wide average of 1.8 cM/Mbp. No phenotypic effect mapped to the middle F_{st} peak.

To determine whether the flower color phenotypes reflect variation in gene expression levels, we performed RNAseq on flower buds from homozygous progeny of individuals used in the genetic mapping experiments. Two of fifteen genes detected in the *ROS-EL* region showed highly significant expression differences (Fig. 4*I*, q < 0.001; *SI Appendix*, Fig. S6). One transcript derived from *ROS1* and was about 10 times more abundant for samples with a dominant *ROS* allele compared with those with recessive *ros*, consistent with *ROS* conferring strong magenta. The second differential transcript encoded a *MYB*-like transcription factor with 57% protein identity to *ROS1* in the MYB domain and mapped to the *EL* region (*SI Appendix*, Figs. S5 and S6). This *EL-MYB* was expressed about threefold more in samples with a dominant *EL* allele compared with those with recessive *el*, consistent with it being a repressor of magenta pigmentation (*SI Appendix*, Fig. S6C). These results indicate that *EL* encodes a *MYB*-like transcription factor and show that at least some of the differences in gene activity are transcriptional. The *EL-MYB* gene maps to the rightmost F_{st} peak (Fig. 4*A*). Two other transcripts showed differences in expression between *el*

and *EL* genotypes (genes 5 and 14, Fig. 4*I*, q < 0.01, q < 0.05, respectively) but showed a much weaker correlation with genotype than the *EL-MYB* gene (*SI Appendix*, Fig. S6 *B* and *C*).

We also analyzed recombinants, termed *ROS1**, with breakpoints just downstream of the *ROS1* gene (Fig. 4*H*). *ROS1** is expressed at a similar level to *A.m.pseudomajus ROS1*, although it carries the *ROS1* coding and upstream region of *A.m.striatum* (*SI Appendix*, Fig. S6C). Thus, variation in *ROS1* transcript levels largely maps to a downstream enhancer. The paler flowers of *ROS1** compared with *A.m.pseudomajus ROS1* (Fig. 1*E* vs. Fig. 1*H*) suggests that variation in the coding region also contributes to the phenotype. Taken together with the observation of low π_w for only the left and right F_{st} peaks, these findings suggest that selective sweeps at *ROS* and *EL* caused these F_{st} peaks.

Gene Flow Lowers F_{st} Outside the *ROS/EL* Region. Sequence pools for populations of *A.m.pseudomajus* and *A.m.striatum* away from the center of the hybrid zone (~20 km apart instead of ~2.5 km) showed a higher median F_{st} (0.048 ± 0.0008 compared with 0.040 ± 0.0004) and more variable profile for chromosome 6 than for nearby populations (Figs. 2 *H* and *I*, 3*B*, and 5). By contrast, F_{st} values at *ROS*, *EL*, and the intervening region were similar to
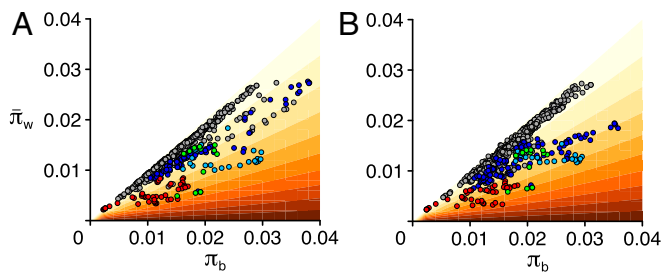
Fig. 3. Comparison of within- and between-population divergence in the *ROS/EL* region. Relationship between π_b and π_w for pools sampled either side of the hybrid zone, separated by ~2.5 km (*A*, YP1 and MP2, corresponding to Fig. 2 *B* and *C*) or ~20 km (*B*, YP4 and MP11, corresponding to Fig. 2 *H* and *I*), summarized in 10-kb windows, with a color gradient indicating the respective F_{st} (light colors, low; dark colors, high). The left, middle, and right F_{st} peaks indicated in Fig. 2*C* are shown as red, light blue, and green points, respectively. The dark blue points indicate windows between those F_{st} peaks. Other windows from around the *ROS* region are shown in gray.

those for the nearby populations (Figs. 2 *H* and *I* and 5). More remote populations showed a further increase in F_{st} for chromosome 6, with some comparisons yielding numerous F_{st} peaks, so that those at *ROS* and *EL* no longer stood out (Figs. 2 *J* and *K* and 5 and *SI Appendix*, Fig. S3 *A* and *D* and Table S9). Such a pattern of "isolation by distance" is often seen and indicates that gene flow reduces local divergence. In contrast, F_{st} is elevated across the whole *ROS/EL* region (Fig. 5), as expected from a strong barrier to gene flow generated by selection on *ROS* and *EL* (28). The statistical significance of these patterns is considered in *SI Appendix, Supplementary Text S1.3*.

A barrier to gene flow is also expected to cause sharp clines at any loci within it, regardless of whether they are selected. Indeed, we observe sharp clines at all divergent SNPs within or near the genomic islands, including those that lie outside *ROS* or *EL* (Fig. 2*L* and *SI Appendix, Supplementary Text S2 and Fig. S7*). Of the ~6 × 10⁵ biallelic SNPs on chromosome 6, 115 showed frequency differences greater than 0.8 between the outer pools (~20 km apart). One hundred and one of these differential SNPs were within an ~0.5 Mbp *ROS/EL* region (Fig. 2*M* and *SI Appendix*, Fig. S3*C*), 14 of which were within the *ROS* and *EL* F_{st} peaks, 74 were between these peaks, and 13 were in flanking regions. Comparing SNP allele frequencies in the pools showed that the 14 differential SNPs within the *ROS* and *EL* F_{st} peaks, together with most of the 74 SNPs from the intervening region, exhibited clines centered at the hybrid zone (Fig. 2 *N* and *O*), confirmed and further refined by individual genotyping (Fig. 2*L* and *SI Appendix*, Fig. S7). The remaining differential SNPs, including 14 that were distributed sparsely along the chromosome (Fig. 2*M*), mainly showed a frequency change over a geographic region where the population density is low (Fig. 2*P* and *SI Appendix*, Fig. S7*C*). The change in frequency for these SNPs likely reflects fluctuations caused by the reduced gene flow created by the population density gap.

These findings support the hypothesis of a selective barrier at the *ROS/EL* region. The yellow flower patterning gene *SULF* exhibits steep SNP clines centered at the same geographical location as *ROS-EL* clines (12), supporting the idea that selection on flower color is the basis of the barrier.

Based on the 0.5-cM distance between *ROS* and *EL*, recombinants should be generated at hybrid zones, at a rate of 0.5% per heterozygote. Genotyping 2,393 individuals at the hybrid zone, using haplotype-specific markers in *ROS1* and *EL*, identified 201 recombinant haplotypes, which reached ~10% frequency at the center of the hybrid zone (Fig. 4 *J* and *K*). Genotyping and test-crossing of progeny grown from 27 recombinants confirmed that most gave the expected phenotypes (*SI Appendix, Supplementary Text S3*). Assuming a neutral model with no selection against recombinants, we estimated a lower bound of ~85 generations for the age of this hybrid zone (*SI Appendix, Supplementary Text S4*). If the hybrid zone is older than this, then selection must have acted to eliminate recombinants. A
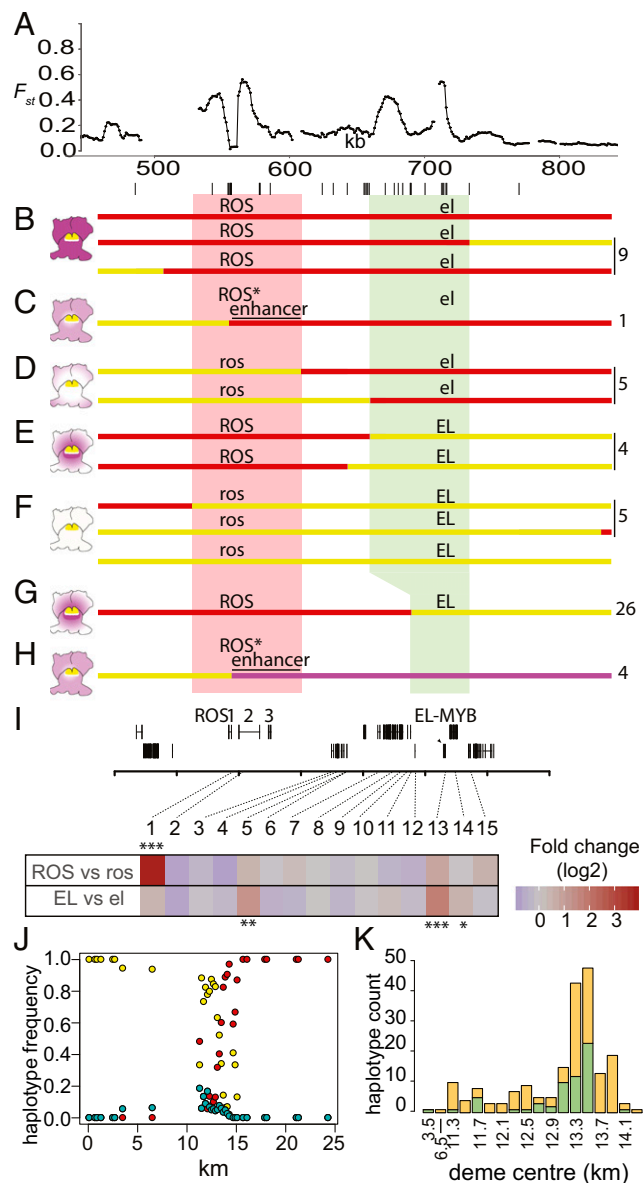

Fig. 4. Mapping loci in relation to F_{st} peaks. (*A*) F_{st} profile for pools in Fig. 2*B* (YP1 vs. MP2) showing location of genes and markers (lines below) used for mapping. (*B–H*) Mapping *ROS* and *EL*. Pale red and pale green boxes indicate mapping intervals for *ROS* and *EL*, respectively. Parental haplotypes shown as lines in red (*A. majus* JI7), magenta (*A.m.pseudomajus*), or yellow (*A.m.striatum*). Recombination to the left and right of the F_{st} peak gives parental phenotypes (*B* and *F*); recombination 3′ of *ROS1* gives pale magenta (*C* and *H*); recombination between *ROS* and *EL* gives very pale (*D*) or restricted (*E*) patterns. Numbers of each class recovered shown, *Right*. (*I*) Floral bud expression of 15 genes found in or between the *ROS* and *EL* mapping intervals. Significant differential expression for *ROS* vs. *ros* or *EL* vs. *el* comparisons at *q* (false discovery rate) < 0.05, *q* < 0.01, and *q* < 0.001 is indicated by one, two, or three asterisks, respectively. Only genes with a mean expression of >5 transcripts per million are shown. The sole gene in the region with significant differential expression in *ROS* vs. *ros* comparisons was *ROS1* (*q* < 5.6e⁻²⁹). *EL-MYB* showed the most significant differential expression in the *EL* vs. *el* comparison (*q* < 2.3e⁻⁹) with two further genes (Gene 5, which is outside the mapped *EL* interval) and Gene 14, which is immediately adjacent to *EL-MYB*) reporting differential expression at lower significance thresholds. (*J*) Frequency of *A.m.pseudomajus* (magenta), *A.m.striatum* (yellow), and recombinant (turquoise) haplotypes in demes with ≥8 individuals along the hybrid zone transect. (*K*) Barplot showing counts of recombinant haplotypes for all demes with ≥8 individuals (*rosˢ elᴾ* in green; *ROSᴾ ELˢ* in orange). Deme center locations between 11.3 and 14.3 km are at 0.2-km intervals. For details of genotyping, see *SI Appendix, Supplementary Text S3*.
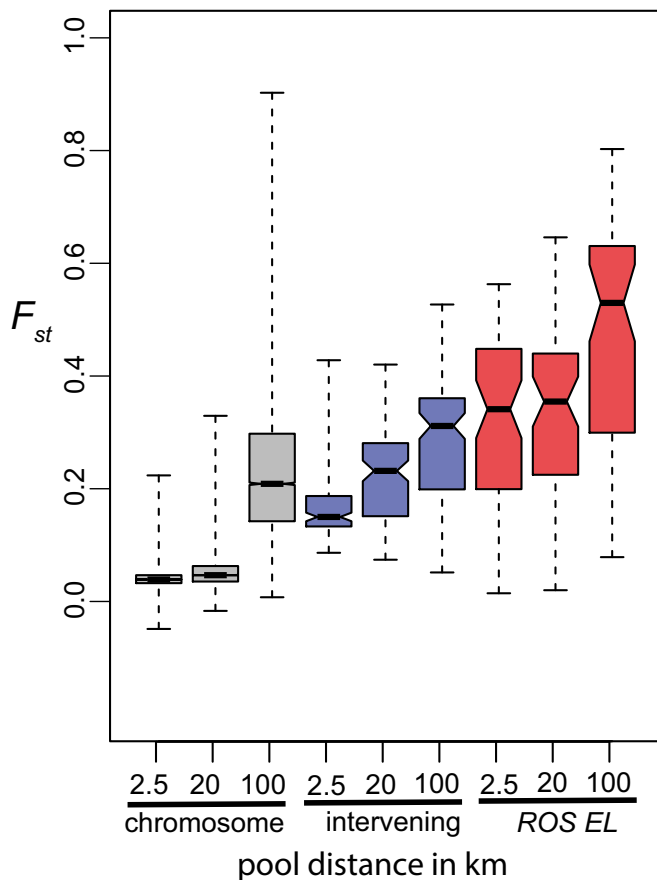
Fig. 5. Relative divergence between populations at different geographic locations. Notched boxplots of F_{st} for three genomic regions: chromosome 6 (gray, from position >35 Mb excluding the *ROS/EL* region), interval between *ROS* and *EL* (blue), and the *ROS* and *EL* loci (pink). For each boxplot: the horizontal waistline indicates the median, the point indicates the mean, the length of the waist indicates the 95% confidence interval of the median, the box indicates the interquartile range, and the whiskers extend to the data minima and maxima. For each genomic region, three *A.m.striatum/A.m.pseudomajus* comparisons are shown, separated by 2.5 km (YP1 and MP2), 20 km (YP4 and MP11), or 100 km (ML-CIN). Distributions are based on values calculated for 10-kb windows, 1-kb step size. Windows overlying *ROS* and *EL*: midpoints 530–575 kb and 707–720 kb on *ROS* scaffold. Windows between *ROS* and *EL*: midpoints 576–706 kb on *ROS* scaffold.

note attached to a herbarium specimen of *A.m.pseudomajus* from 1928 (London Natural History Museum) describes extensive color polymorphism at the geographic location of the hybrid zone, further suggesting that the hybrid zone is at least 90 y old.

The barrier to gene flow observed at *ROS/EL* raises the question of whether this alone could be responsible for the F_{st} peaks. According to this view, the drop in F_{st} in the intervening region between the peaks would be due to gene flow. However, selection at two linked loci (*ROS* and *EL*) generates a strong barrier to gene flow throughout the intervening region because two recombination events are required to transfer a neutral allele onto the opposite genetic background (*SI Appendix, Supplementary Text S5* and Figs. S15 and S16). A barrier of this form would therefore not be expected to generate two separate sharp peaks in F_{st}, as is observed. Thus, the barrier to gene flow alone cannot be responsible for the two sharp F_{st} peaks. This argument illustrates the value of having two linked loci for distinguishing hypotheses. A further advantage of having two linked loci is that it allows a region of elevated F_{st} to be readily picked out because the barrier extends over 0.5 cM and >200 kb. Single selected loci would generate a barrier over a narrow region, which would be harder to detect.

The observation that flower color variation under selection derives from two closely-linked loci (*ROS* and *EL*) seems to lend support to the idea that divergent loci tend to cluster because linkage hinders swamping of locally adapted alleles (5, 29). However, other pigment loci under selection (e.g., *SULF*) are unlinked to *ROS* and *EL*, showing that tight linkage is not essential. Moreover, *ROS* and *EL* are both MYB-like transcription factors and so may be clustered due to gene duplication. Thus, clustering may not be due to selection for linkage (*SI Appendix, Supplementary Text S1.6*).

Role of Selective Sweeps and Barriers to Gene Flow in Generating Genomic Islands. Taken together, the clines, genetic analysis, transcriptional differences, and analysis of F_{st} peaks indicate that the *ROS/EL* genomic island and its surround have been shaped by two processes: (*i*) historic selective sweeps that led to different *ROS* and *EL* alleles becoming fixed in *A.m.pseudomajus* and *A.m.striatum* populations and (*ii*) selection against hybrid genotypes generated
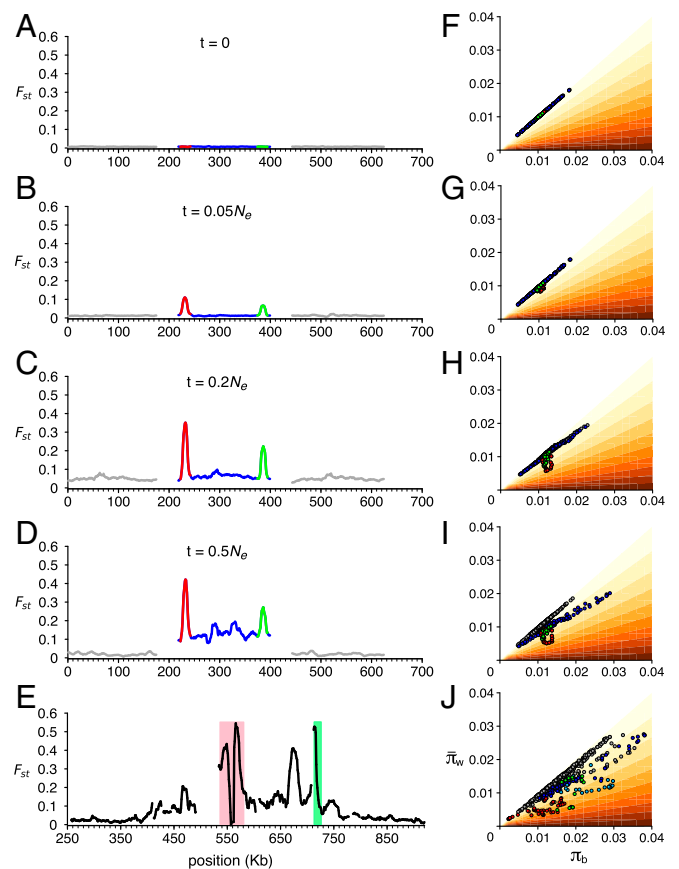

Fig. 6. Simulations of gene flow and selective sweeps. Combined effects of a barrier to gene flow and selective sweeps on F_{st} (*Left*) and on π_b and π_w (*Right*). (*A* and *F*) A homogeneous population is split by a geographic barrier. (*B* and *G*) Alleles at *ROS* and *EL* (red, green) sweep through the separate populations, reducing diversity, π_w, generating peaks in F_{st}. (*C* and *H*) Further sweeps occur at *ROS* and *EL*, strengthening the F_{st} peaks. By $t = 0.2\ N_e$ generations, divergence has increased genome-wide, with $F_{st} \sim 0.05$. At this time, the divergent populations meet and exchange genes everywhere except between *ROS* and *EL*. (*D* and *I*) By time $0.5\ N_e$, F_{st} outside *ROS/EL* has decreased due to mixing (*Left*, black), but has increased between *ROS* and *EL* (*Left*, blue). Although in this scenario, population contact was established at $0.2\ N_e$, similar final profiles for F_{st}, π_b, and π_w would be generated, with contact being made earlier or later than this. (*E* and *J*) The π_b, π_w observed in pools YP1, MP2, 2.5 km apart, with the maximum F_{st} observed at *ROS* indicated by pale red (*E*) or red (*J*), and at *EL* indicated by green. Note that N_e is estimated as roughly 8.3×10^4 (*SI Appendix, Supplementary Text S1.3*). For further details, see *SI Appendix, Supplementary Text S1.5*.

where *A.m.pseudomajus* and *A.m.striatum* populations meet, creating a local barrier to gene flow (28). We performed simulations to explore scenarios consistent with the data and modes of selection.

To provide constraints on simulations, we first estimated the age of the selective sweeps. Based on the residual diversity within the sharp peaks at *ROS* and *EL*, we estimated the date of the most recent sweeps to be ~90,000 generations ago (*SI Appendix, Supplementary Text S1*); this is an upper bound, since "soft sweeps" might not have eliminated all diversity. We also estimated the age of the barrier to gene flow. As detailed in *SI Appendix, Supplementary Text S1*, the time required for F_{st} in the *ROS/EL* interval to accumulate to the observed value of 0.125 is $T \sim 0.54\ N_e \sim$ 45,000 generations (where N_e = effective population size). Thus, both estimates suggest that selective sweeps and a barrier to gene flow were established roughly $N_e \sim 10^5$ generations ago.

We assume that a homogeneous ancestral population is first split by a geographic barrier, allowing sweeps to occur independently in each population (Fig. 6 *A* and *F*, for simplicity assuming an initial $F_{st} \sim 0.0$). Geographic separation is a simple way of ensuring that alleles swept in one population do not sweep into the other, although other scenarios such as environmental heterogeneity are possible; the sequence data are also compatible with divergence in primary contact. Sweeps at *ROS* and *EL* (red, green in Fig. 6 *B* and *G*) reduce diversity, π_w, generating peaks in F_{st}. These sweeps presumably reflect the selective advantage of a change in flower color, compared with the ancestral phenotype in each population. Given that both populations underwent sweeps, the ancestral flower phenotype would have been different from both of the current phenotypes in *A.m.pseudomajus* or *A.m.striatum*. Further sweeps at *ROS* and *EL* strengthen the F_{st} peaks (Fig. 6 *C* and *H*). Unlike the simulations, in real populations, it is possible that global and/or local sweeps occur at many other genetic loci and spatial locations, in addition to *ROS* and *EL*, creating a more rugged F_{st} profile across the genome.

After a period of time (0.2 N_e generations in the simulation shown in Fig. 6), the divergent populations come into contact. Gene flow leads to a lowering of F_{st} from the chromosome-wide average, except at loci where a barrier has been established. We propose that a barrier to gene flow occurs for only a subset of swept loci: those for which epistatic interactions or frequency dependence maintain divergence. *ROS* and *EL* represent one such case, as their interactions, together with loci controlling yellow, lead to alternative floral guides. Other loci that underwent sweeps, but led to no incompatibility (presumably the majority of sweeps) would undergo

gene flow, with the allele conferring higher overall fitness going to fixation in both populations. By time 0.5 N_e, F_{st} outside *ROS/EL* has decreased due to gene flow (gray), but has further increased between *ROS* and *EL* (blue) because of the local barrier to gene flow (Fig. 6 *D* and *I*). The resulting F_{st}, π_b, and π_w values are comparable to those observed (compare Fig. 6 *D* and *I* with Fig. 6 *E* and *J*). According to the above scenario, selective sweeps led to fixation of different alleles in each population, and selection maintains a local barrier to gene flow. Multiple changes in alleles are involved, a reasonable assumption given these events occurred over a period of ~10^5 generations, extending over glacial periods, during which populations and the environment were in a state of flux.

Our analysis indicates that both selective sweeps and barriers to gene flow combine to shape genomic islands of differentiation. The barrier to gene flow at *ROS/EL* is insufficient to prevent exchange for much of the genome. However, if the barrier were more severe and applied to additional loci, it could prevent gene flow more completely, leading to speciation. The mechanisms that created the genomic islands may therefore represent partial steps toward reproductive isolation and speciation.

Materials and Methods

Full details of plant material, DNA extraction, genome sequence analysis, population genomics, genotyping, SNP analysis for geographic, and RNAseq analysis are given in *SI Appendix, Materials and Methods*. Details on inferences from pairwise diversity and divergence, geographic cline analysis, and genotypic screens are given in *SI Appendix*. Genomic sequence datasets are available at European Nucleotide Archive (ENA) with accession number PRJEB28287, and RNAseq datasets are deposited in National Center for Biotechnology Information (NCBI) Gene Expression Omnibus (GEO) with accession number GSE118621. Associated scripts are provided at linked public data repositories as detailed in *SI Appendix, Materials and Methods*, and further information on the hybrid zone is available at www.antspec.org.

1. Hohenlohe PA, et al. (2010) Population genomics of parallel adaptation in threespine stickleback using sequenced RAD tags. *PLoS Genet* 6:e1000862.
2. Martin SH, et al. (2013) Genome-wide evidence for speciation with gene flow in Heliconius butterflies. *Genome Res* 23:1817–1828.
3. Poelstra JW, et al. (2014) The genomic landscape underlying phenotypic integrity in the face of gene flow in crows. *Science* 344:1410–1414.
4. Clarkson CS, et al. (2014) Adaptive introgression between Anopheles sibling species eliminates a major genomic island but not reproductive isolation. *Nat Commun* 5:4248.
5. Ellegren H, et al. (2012) The genomic landscape of species divergence in Ficedula flycatchers. *Nature* 491:756–760.
6. Pennisi E (2014) Disputed islands. *Science* 345:611–613.
7. Cruickshank TE, Hahn MW (2014) Reanalysis suggests that genomic islands of speciation are due to reduced diversity, not reduced gene flow. *Mol Ecol* 23:3133–3157.
8. Ma T, et al. (2018) Ancient polymorphisms and divergence hitchhiking contribute to genomic islands of divergence within a poplar species complex. *Proc Natl Acad Sci USA* 115:E236–E243.
9. Wolf JB, Ellegren H (2017) Making sense of genomic islands of differentiation in light of speciation. *Nat Rev Genet* 18:87–100.
10. Charlesworth B, Nordborg M, Charlesworth D (1997) The effects of local selection, balanced polymorphism and background selection on equilibrium patterns of genetic diversity in subdivided populations. *Genet Res* 70:155–174.
11. Whibley AC, et al. (2006) Evolutionary paths underlying flower color variation in Antirrhinum. *Science* 313:963–966.
12. Bradley D, et al. (2017) Evolution of flower color pattern through selection on regulatory small RNAs. *Science* 358:925–928.
13. Hackbarth J, Michaelis P, Scheller G (1942) Untersuchungen an dem *Antirrhinum*-Wildsippen-Sortiment von E. Baur. *Z Indukt Abstamm Vererbungsl* 80:1–102.
14. Schwinn K, et al. (2006) A small family of MYB-regulatory genes controls floral pigmentation intensity and patterning in the genus Antirrhinum. *Plant Cell* 18:831–851.
15. Stubbe H (1966) *Genetik und Zytologie von Antirrhinum L. sect. Antirrhinum* (Veb Gustav Fischer Verlag, Jena, Germany).
16. Khimoun A, et al. (2012) Ecology predicts parapatric distributions in two closely-related Antirrhinum majus subspecies. *Evol Ecol* 27:51–64.
17. Shang Y, et al. (2011) The molecular basis for venation patterning of pigmentation and its effect on pollinator attraction in flowers of Antirrhinum. *New Phytol* 189:602–615.
18. Gegear RJ, Laverty TM (2005) Flower constancy in bumblebees: A test of the trait variability hypothesis. *Anim Behav* 69:939–949.
19. Smithson A, Macnair MR (1996) Frequency-dependent selection by pollinators: Mechanisms and consequences with regard to behaviour of bumblebees Bombus terrestris (L.) (Hymenoptera: Apidae). *J Evol Biol* 9:571–588.
20. Oyama RK, Jones KN, Baum DA (2010) Sympatric sister species of Californian Antirrhinum and their transiently specialized pollinators. *Am Midl Nat* 164:337–347.
21. Counterman BA, et al. (2010) Genomic hotspots for adaptation: The population genetics of Müllerian mimicry in *Heliconius erato*. *PLoS Genet* 6:e1000796.
22. Mallet J, Barton NH (1989) Strong natural selection in a warning-color hybrid zone. *Evolution* 43:421–431.
23. Joron M, Mallet JL (1998) Diversity in mimicry: Paradox or paradigm? *Trends Ecol Evol* 13:461–466.
24. Jiggins CD (2017) *The Ecology and Evolution of Heliconius Butterflies* (Oxford Univ Press, Oxford).
25. Nadeau NJ, et al. (2012) Genomic islands of divergence in hybridizing Heliconius butterflies identified by large-scale targeted sequencing. *Philos Trans R Soc Lond B Biol Sci* 367:343–353.
26. Schlötterer C, Tobler R, Kofler R, Nolte V (2014) Sequencing pools of individuals–Mining genome-wide polymorphism data without big funding. *Nat Rev Genet* 15:749–763.
27. Payseur BA, Rieseberg LH (2016) A genomic perspective on hybridization and speciation. *Mol Ecol* 25:2337–2360.
28. Barton N, Bengtsson BO (1986) The barrier to genetic exchange between hybridising populations. *Heredity (Edinb)* 57:357–376.
29. Yeaman S, Aeschbacher S, Bürger R (2016) The evolution of genomic islands by increased establishment probability of linked alleles. *Mol Ecol* 25:2542–2558.

EVOLUTION